JOURNAL OF APPLIED ELECTROCHEMISTRY 13 (1983) 221–233

The role of sintering time on reversibility of Ni(s)–NiO(s) electrodes for high temperature solid oxide electrolyte galvanic cells

D. GOZZI, P. L. CIGNINI*

Istituto di Chimica Fisica, Università di Roma, P. 1e Aldo Moro, 5 – 00185 Roma, Italy

Received 5 July 1982

The reversibility of solid electrolyte galvanic cells such as

$$Mo/Ni(s)\text{–}NiO(s)/CSZ/Fe(s)\text{–}Fe_{1-\delta}O(s)/Mo$$

has been studied with respect to the sintering time of the active powders. Pellets from short (7h) and long (14h) sintering times have been prepared and assembled to give the above cells. Each of them has been thermally cycled and only the cells containing Ni(s)–NiO(s) electrodes prepared with a long sintering time give emf versus T curves which are independent of cycle. These values are in close agreement with the literature.

For the cell reaction

$$NiO(s) + (1-\delta)Fe(s) = Ni(s) + Fe_{1-\delta}O(s)$$

the free energy change

$$\Delta G = -(27.85 \pm 0.06) - (0.02157 \pm 0.00004)T \text{ kJ mol}^{-1}$$

has been found in the temperature range 977–1350 K.

To check the electrochemical reversibility, cyclic voltammetry has also been used. On the basis of these results and of SEM analysis of the electrode pellets, a mechanism is proposed whereby only at long sintering time would a triple phase contact at the electrode/electrolyte interface be produced.

1. Introduction

For some years solid electrolyte galvanic cells have been used both for determining thermodynamic quantities of inorganic materials at high temperatures and when the solid electrolyte is an oxide, as oxygen sensors to detect oxygen in gas mixtures or in fused metals.

Several papers, books and reviews [1–6] have been published on those applications of solid electrolytes together with their potentialities and limitations [7–11].

Of course, reversibility should be the main requirement of a galvanic cell which is obtainable only if both the electrodes are reversible, i.e., they simultaneously exchange electrons and ions as a source and a sink of electrons and ions without changing their electrode potential (ideally non-polarizable electrode). This implies that electron transfer processes at the interfaces occur with the same rates as mass transfer within the electrolyte and in the electrodes from the electrolyte/electrode interface toward the bulk and vice versa. Secondly, the measured cell emf will be as predicted by the free energy change of the virtual cell reaction if the electrolyte works in its own electrolytic domain [7, 12], if mixed potentials are absent at electrolyte/electrode interfaces and if no chemical transformation occurs at these phase boundaries, i.e., the materials of the electrode phase do not react either among themselves or with the electrolyte phase.

$Me(s)\text{–}Me_xO_y(s)$ mixture electrodes are generally used in solid oxide electrolyte galvanic cells

* Researcher of the Centro di Termodinamica Chimica alle Alte Temperature of National Research Council (CNR) c/o Istituto di Chimica Fisica, Università di Roma.

0021–891X/83/020221–13$04.06/0

especially in oxygen sensors as, for instances, Fe(s)–$Fe_{1-\delta}O$(s), Cr(s)–Cr_2O_3(s), Ni(s)–NiO(s), Mo(s)–MoO_2(s), Nb(s)–NbO(s), etc. which should behave as reversible electrodes able to fix the oxygen chemical potential at one of the interfaces (oxygen chemical potential reference).

Many examples of application of these electrodes can be found in the literature and it is known that only a few of them really behave as reference electrodes without special precautions during preparations.

According to the literature [13, 14] the Fe(s)–$Fe_{1-\delta}O$(wüstite) mixture certainly belongs to that category while for the Ni(s)–NiO(s) mixture, different and contradictory information is reported [15–18]. Probably, this is because of different methods of preparation of the mixture, as it is well known that many experimental parameters may influence its final properties. For example, one could separately study the effect of the powder grain size, their size distributions, porosity, mixing, temperature, oxygen partial pressure and time of sintering. If pellets are considered, moulding pressure and the extent of final surface polishing should probably also be taken into account.

The scope of the present work is that to show how a change of one of those parameters can affect the behaviour of the Ni(s)–NiO(s) electrode without appreciably modifying the properties of Fe(s)–$Fe_{1-\delta}O$(s) electrode.

2. Procedure

The procedure adopted in preparing the Ni(s)–NiO(s) and Fe(s)–$Fe_{1-\delta}O$(s) pellets is based on keeping constant all the above mentioned parameters except the sintering time. In fact, in order to approach the general problem, this parameter is the easiest to control.

Two sintering times, 7 and 14 hours, have been arbitrarily selected. For each of the two electrode mixtures, we have used two kinds of sintered pellets: at long, l, and short, s, sintering time. With these pellets, galvanic cells of type 1 can be assembled

$$\underset{\text{pellet}}{\mathrm{Mo/Me^{I}\text{–}Me^{I}_{x}O_{y}/CSZ/Me^{II}\text{–}Me^{II}_{x}O_{y}/Mo}}\quad\underset{\text{pellet}}{} \qquad (1)$$

Cells could be constructed by combining the N_l, N_s, I_l, I_s electrode pellets, where N and I stand, respectively, for Ni(s)–NiO(s) and Fe(s)–$Fe_{1-\delta}O$(s). We labelled three types of cells: α, β, γ. Cells with (N_l–N_s), (I_l–I_s) electrodes are α cells (symmetrical) while (N_l–I_l), (N_s–I_s) and (N_s–I_l), (N_l–I_s) cells respectively belong to β and γ types.

We only studied β and γ cells by assembling the double cells

$$\begin{array}{l}\mathrm{Mo/N_l/CSZ/I_l/Mo/N_s/CSZ/I_s/Mo} \\ \mathrm{+ - - -}\,E_\beta\,\mathrm{- - - + - - -}\,E'_\beta\,\mathrm{- - - +}\end{array} \qquad (2)$$

and

$$\begin{array}{l}\mathrm{Mo/N_s/CSZ/I_l/Mo/N_l/CSZ/I_s/Mo} \\ \mathrm{+ - - - -}\,E_\gamma\,\mathrm{- - + - - -}\,E'_\gamma\,\mathrm{- - - +}\end{array} \qquad (3)$$

respectively. In this way, each pair of cells was in the same environment and followed the same thermal cycle. In two separate series, each of three runs for cells 2 and 3, emf values, E and E', were measured alternatively, as a function of a step-wise temperature programme.

To check electrochemical reversibility, cells 2 and 3 were subjected to triangular wave voltametry (TWV).

3. Experimental procedure

3.1. *Preparation of electrode pellets*

In Table 1 are reported the experimental conditions adopted in preparing sintered electrode pellets. The metal/oxide ratios were selected according to the most frequent values found in the literature. Wüstite was prepared by mixing iron and iron oxide (Fe_2O_3) in the molar ratio 1 : 1 and reacted in an iron crucible at 1573 K overnight. All the metal and oxide powders were sieved and only the fraction going through a 325 mesh sieve was used.

Metals and oxides were all of stated purity, 99.99%, from Cerac (USA). Powder mixtures were obtained by intimate dry mixing of the respective metal and oxide powders in the given weight ratio. Pellet moulding was performed cold in a 6 mm diameter stainless steel die by increasing the pressure step-wise.

3.2. *Electrolyte*

Electrolytes used were Zircoa (USA) pellets of ZrO_2 with 15 mol% of CaO(CSZ), 6 mm diameter

Table 1. Experimental conditions adopted in preparing the sintered electrode pellets

Electrode pellet	$N_{l,s}$	$I_{l,s}$
MeO content (wt%)	9.1	23.1
Me and MeO grain size (mesh)	>325	>325
Moulding pressure (MPa)	620	620
Dimensions (mm) diameter × thickness	6 × 3–5	6 × 3–5
P_{O_2} of sintering (mPa)	<0.1	<0.1
Temperature of sintering (K)	1268	1259
Final polishing diamond paste (μm)	0–2	0–2

× 1.6 mm thick obtained by reducing their original diameter of 12.7 mm by diamond tools. Before use, all electrolyte pellets were heated in air at 1273 K for a day.

3.3. *Apparatus*

In order to obtain an argon stream with a low and controlled level of oxygen, argon with an initial content of 5 ppm of oxygen was purified according to the procedure previously described [19].

Assembly of cells 2 and 3 and the related construction details have been already reported [19].

Both the sintering of the electrode pellets and emf measurements were carried out in a static atmosphere of dry and carefully purified argon. Before any experiment, the furnace was evacuated for a long time at a pressure of 1.10^{-4} Pa, first at room temperature and then while heating to 500 K. Then the furnace was cooled and purified argon was let into the furnace, after which the apparatus was heated to the temperature of the experiments.

The rate of temperature changes throughout was 5 K min^{-1} while temperature was measured by a Pt/Pt, Rh10% thermocouple and continuously recorded with an accuracy of ± 1 K.

E and E' emfs of each of the double cells, 2 and 3, were alternatively measured by an automatic device which switched, at set intervals, the extreme leads of those cells with one of the floating differential inputs of the electrometer (Amel 631, Italy). The common lead was connected to the other electrometer input. The emfs were continuously recorded with a total accuracy of ± 0.1 mV.

TWV curves were recorded on a X, Y recorder with abscissa controlled by an analogic function generator (Amel 565, Italy) and ordinate controlled by the output of a potentiostat (Amel 556, Italy) which is driven by the function generator. The accuracy of presetting both the initial voltage and vertices values of TWV was ± 0.2 mV.

In order to simplify the cell apparatus TWV measurements were performed with a double ended potentiostat by short-circuiting the reference and counter electrode inputs to which Fe(s)–$Fe_{1-\delta}O$(s) electrode was connected.

4. Results

4.1. *Emf measurements*

Figures 1 and 2 show the typical trends of E and E' versus T of cells 2 and 3 while data of cell 2 are given as an example in Table 2.

For each of the two double cells three runs were carried out with fresh pellets of electrodes and electrolyte. This was preferred to using the same cell components in order to check that the behaviour electrode pellets, prepared in the same way (short or long), was reproducible.

From the results listed in Table 3, it is clear that:

The behaviour of each cell is consistent throughout the runs and very similar to Figs. 1 and 2.

Only cells $\beta(N_1–I_1)$ and $\gamma(N_1–I_s)$ behave reversibly since their emf versus T trends are unaffected by the thermal cycle and emf values agree very well with the electrode reactions

$$NiO(s) + 2e = Ni(s) + O^{2-}(CSZ) \qquad (4)$$

at the N/CSZ interface and

$$(1-\delta)Fe(s) + O^{2-}(CSZ) = Fe_{1-\delta}O(s) + 2e \qquad (5)$$

at CSZ/I interface. At zero net current, the following overall cell reaction can be considered:

$$(1-\delta)Fe(s) + NiO(s) = Ni(s) + Fe_{1-\delta}O(s) \qquad (6)$$

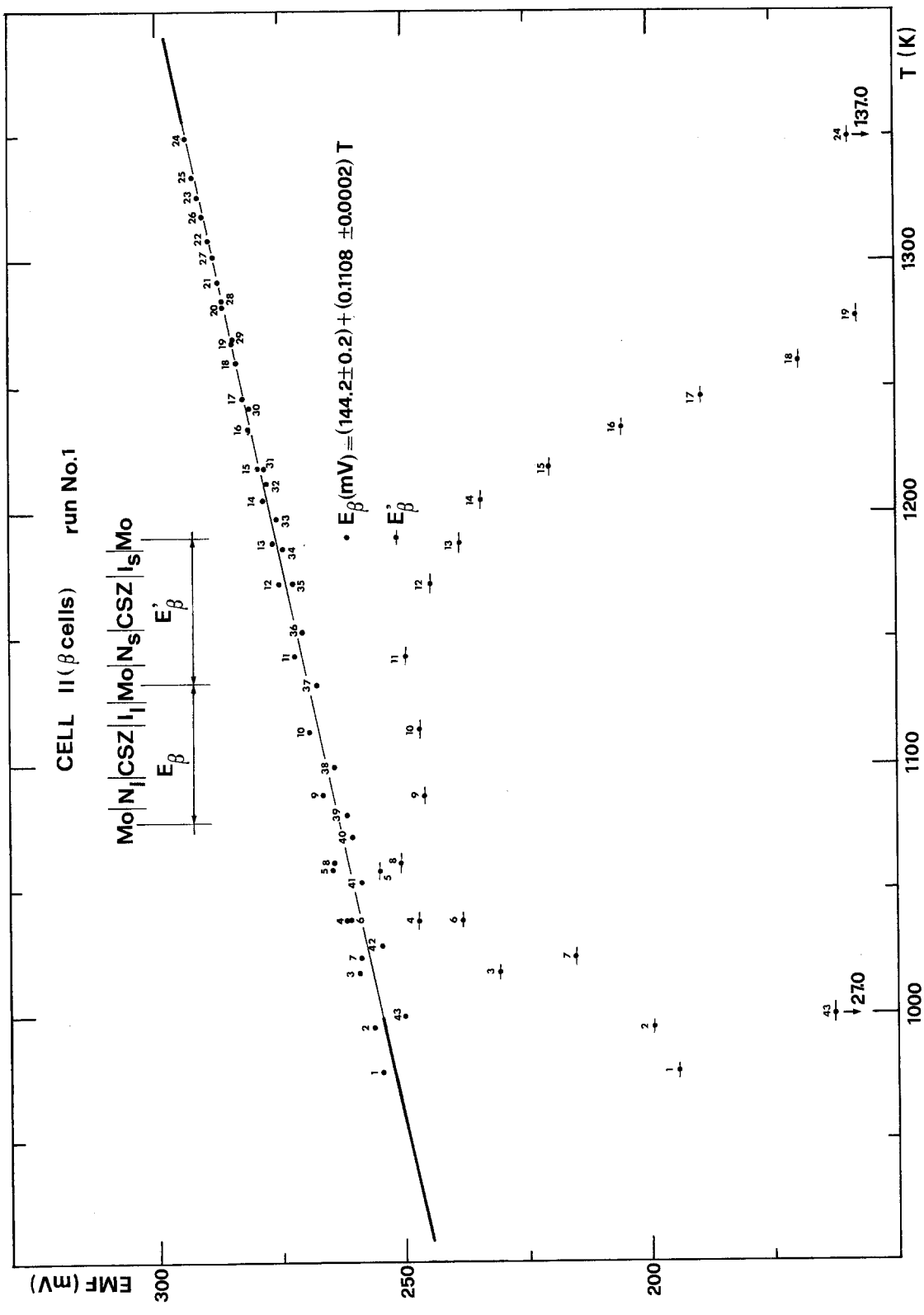

Fig. 1. The emf versus T trends for β cells.

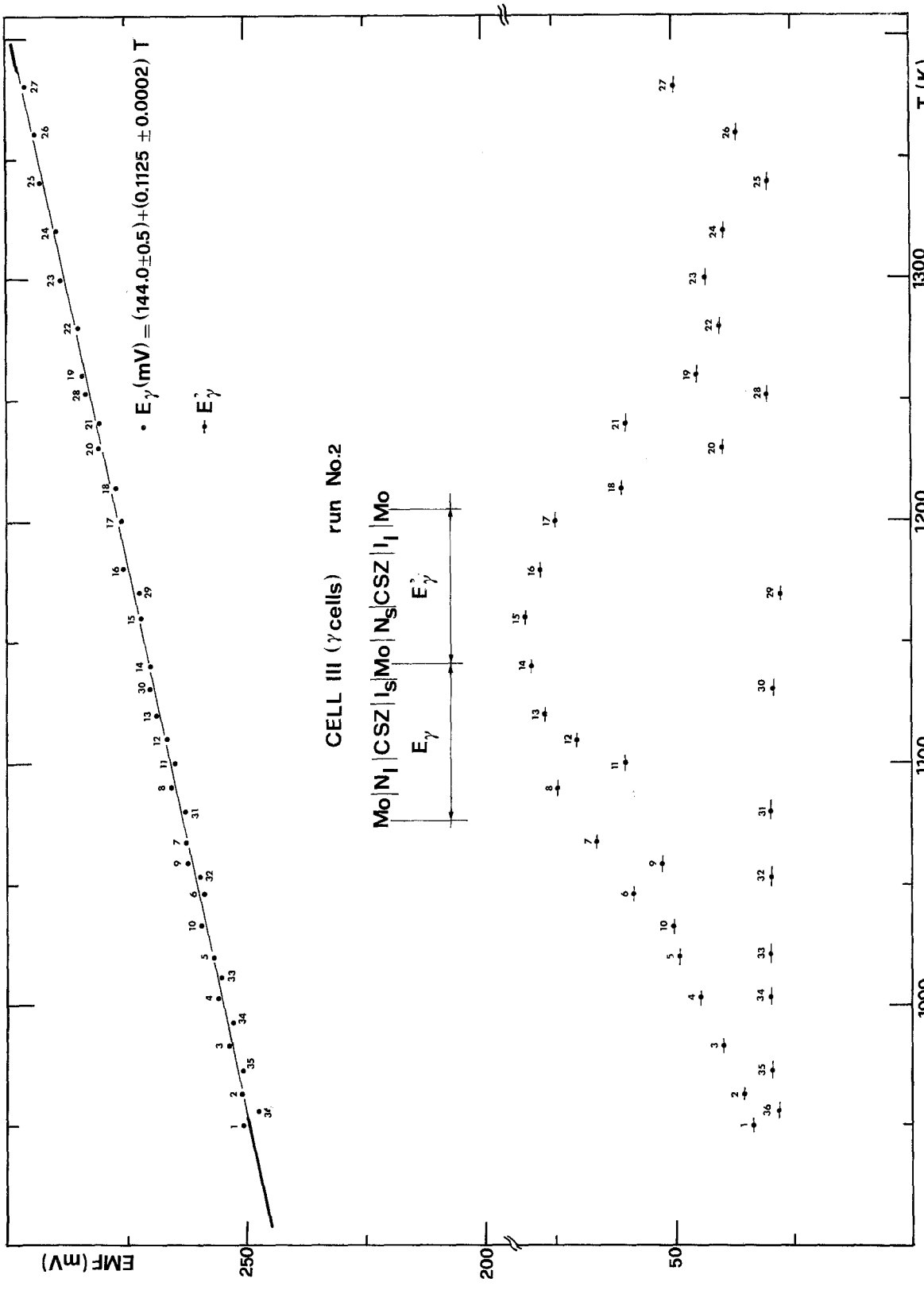

Fig. 2. The emf versus T trends for γ cells.

Table 2. The emf values E_β and E'_β of the double cell 2 containing β cells. E_β refers to $N_I/CSZ/I_I$ cell and E'_β refers to $N_s/CSZ/I_I$. Run no. 1

Points	*T* (K)	E_β (mV)	E'_β (mV)	*Points*	*T* (K)	E_β (mV)	E'_β (mV)
1	977	254.5	194.5	23	1326	291.5	132.4
2	995	256.0	199.6	24	1350	293.9	137.0
3	1017	259.1	230.8	25	1334	292.3	111.0
4	1038	261.6	247.1	26	1318	290.6	91.4
5	1058	264.1	255.0	27	1302	288.6	76.5
6	1038	261.0	238.2	28	1284	286.5	65.1
7	1023	258.8	215.2	29	1269	284.5	–
8	1061	264.0	250.5	30	1242	281.0	–
9	1088	266.4	246.0	31	1218	278.1	–
10	1114	269.2	246.7	32	1212	277.2	–
11	1143	272.1	249.7	33	1198	275.6	41.7
12	1172	275.1	244.3	34	1186	274.1	–
13	1188	276.8	238.7	35	1172	272.4	–
14	1205	278.5	234.1	36	1153	270.3	–
15	1218	279.6	220.2	37	1132	267.7	–
16	1234	281.2	205.4	38	1099	263.9	–
17	1246	282.5	189.2	39	1080	261.7	–
18	1260	283.9	169.5	40	1071	260.5	–
19	1268	284.7	157.8	41	1053	258.4	–
20	1282	286.4	145.0	42	1028	254.8	–
21	1292	287.6	150.0	43	1000	249.6	–
22	1309	289.7	125.3				

whose free energy change, ΔG, is the useful electrical work according to the well known equation

$$\Delta G = -2FE \qquad (7)$$

By assuming the average of the least squares correlations of Table 3, as follows

$$\bar{E}(\text{mV}) = (144.3 \pm 0.3) + (0.1118 \pm 0.0002)T \qquad (8)$$

Equation 7 can be rewritten as

$$\Delta\bar{G} = -(27.85 \pm 0.06) - (0.02157 \pm 0.00004)\,T \text{ kJ mol}^{-1} \qquad (9)$$

In Table 4 are reported, for comparison purposes, some self consistent equations for reaction 6 from the literature.

For $\beta(N_s\text{–}I_s)$ and $\gamma(N_s\text{–}I_I)$ cells no correlation can be calculated since emfs are strongly influenced by the thermal cycle, besides being very far from the expected values.

All E' versus T curves show a maximum around 1150 K, the intensity of which apparently does not seem to follow any logical trend.

Reversible behaviour seems to be a characteristic of the cells containing a long sintered Ni(s)–

Table 3. Resumed data for cells 2 and 3

	Run	*E* (mV)	*E'* (mV)	E'_{max} (mV)	T_{max} (K)
Cell 2	1	$(144.2 \pm 0.2) + (0.1108 \pm 0.0002)T$	nc	249.5	1143
(β cells)	2	$(143.9 \pm 0.3) + (0.1112 \pm 0.0004)T$	nc	158.7	1148
	3	$(145.8 \pm 0.1) + (0.1117 \pm 0.0001)T$	nc	170.2	1153
Cell 3	1	$(141.5 \pm 0.2) + (0.1143 \pm 0.0001)T$	nc	201.0	1152
(γ cells)	2	$(144.0 \pm 0.5) + (0.1125 \pm 0.0002)T$	nc	81.5	1160
	3	$(146.2 \pm 0.4) + (0.1103 \pm 0.0003)T$	nc	97.4	1155

nc = no correlation
$\bar{E}$ (mV) = $(144.3 \pm 0.3) + (0.1118 \pm 0.0002)T$
$\bar{T}_{max}$ = 1152 K

Table 4. Self-consistent free energy change data for reaction 6 according to literature

Author	ΔG (kJ mol^{-1})	$-\Delta G_{1273}$ (kJ mol^{-1})
O. Kubaschewski and C. B. Alcock [20]	$-30.54 - 0.020T$	56.00
I. Barin and O. Knacke [21]	$-29.45 - 0.0199T$	54.79
Su-Il Pyun and F. Müller [22]	$-30.55 - 0.0198T$	55.76
This work	$-27.85 - 0.0216T$	55.31

NiO(s) electrode (N_1), independent of the type of Fe(s)–$Fe_{1-\delta}O$(s) electrodes ($I_{1,s}$).

E and E' emfs were noted at a time when, at constant temperature, the E value was stationary. This generally occurred in 1–2 hours after constant temperature was reached, depending on temperature value; the higher the temperature, the shorter the time necessary to reach a stationary E value.

4.2. *TWV curves*

Typical TWV curves obtained on $\beta(N_1–I_1)$ and $\gamma(N_1–I_s)$ cells are reported in Fig. 3. A slow (2 mV s^{-1}) triangular single sweep changes the working electrode potential from its initial value, E_i, to $(E_i - 100)$ mV then to $(E_i + 100)$ mV. The curves shown refer to a $\gamma(N_1–I_s)$ cell at 1068 K; in the lower curve, Ni(s)–NiO(s) electrode (N_1) acts as working electrode while in the upper curve the electrode leads have been exchanged (working electrode I_1).

Also $\beta(N_s–I_s)$ and $\gamma(N_s–I_1)$ cells have been subjected to the same triangular single sweep and the related curves are given in Fig. 4. As above, they correspond to two different connections of the cell with the same sequence.

To qualitatively distinguish which of the two electrodes in cell $\gamma(N_s–I_1)$ behaves irreversibly, let us examine Fig. 5 where two TWV single sweeps compare a wider cathodic potential range and at a voltage scan rate of 20 mV s^{-1}, ten times greater than that previously adopted in Figs. 3 and 4. In this case the applied potential does not cross the zero level while the curves again refer to an exchange of cell leads with the potentiostat inputs. Therefore, in the lower curve, the working electrode is N_1 and in the upper one, the I_1 electrode.

The comparison of Fig. 3 with Fig. 4 clearly shows how, in this case, the electrochemical reversibility concept is well fulfilled since it is sufficient to apply a few millivolts to the cell at its own equilibrium emf such that the overall emf determining reaction is forced to proceed mostly in only one direction (Fig. 3).

Nothing like this appears in Fig. 4 where in the same applied potential range, no electrochemical process seems to take place.

The curve of Fig. 3, obtained by exchanging electrodes, can be practically superimposed by a 180° rotation confirming that the electrodic reactions are the same.

It is important to point out that the TWV curves shown have not been corrected for the ohmic drop and a superimposition of a resistance polarization, according to Vetter [23], should be also taken into account. Therefore, the peak separation in Fig. 3 will be less than that actually measured, also in Fig. 5. According to Delahay [24], for example, the peak separation should be equal to $2 \times 1.1 \times RT/nF$, i.e., 101 mV at 1068 K, while, the value found is 120 mV. Besides, in the latter case, the cathodic peak potential may be influenced by the polarization of N_1 electrode acting there as a 'reference electrode'.

Therefore, the TWV curves show that the observed irreversible behaviour of the $\beta(N_s–I_s)$ and $\gamma(N_s–I_1)$ cells should be attributed to the N_s electrode.

4.3. *SEM analysis*

Scanning electron microscopy observations of unpolished sections of electrode pellet samples, cut perpendicular to the diameter, are reported in Fig. 6.

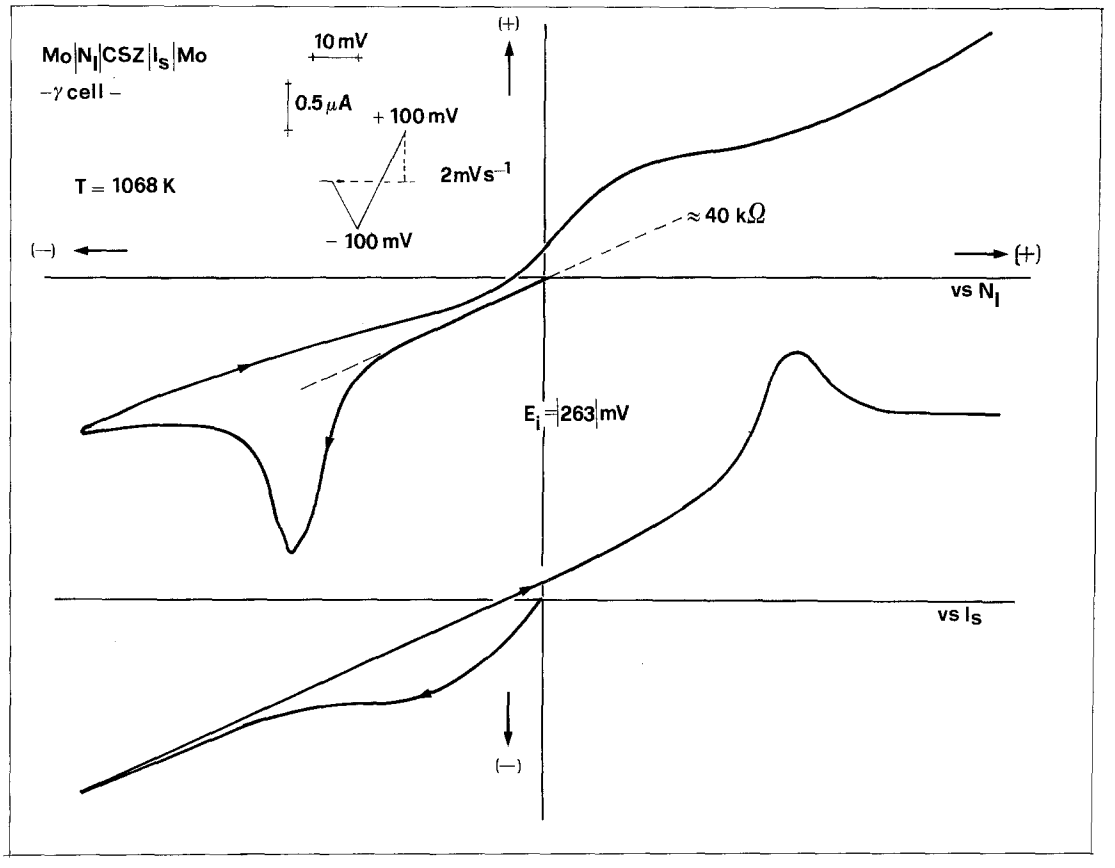

Fig. 3. Typical triangular wave voltammetry curves for a γ cell containing a N_1 electrode.

Comparison of the four types of the investigated pellets (N_1, N_s, I_1, I_s) shows a difference between N samples (Fig. 6a, b) but not between I samples (Fig. 6c, d). In fact, several NiO grains appear in N_1 pellet (Fig. 6b), evenly spread and very well embedded into the metallic framework.

In contrast, in the N_s pellet sample (Fig. 6a), no evidence of such oxide agglomeration appears, even when the magnification was doubled (Fig. 6e).

5. Discussion

As the initial content of NiO is the same in both the N_s and N_1 pellets, the results of SEM analysis are not easy to understand.

A possible explanation is that a NiO grain is completely surrounded by nickel grains owing to a favourable ratio, R, between the number of metal particles and an oxide particle. In fact, by simple calculations, one obtains that

$$R = \left(\frac{100 - w}{w}\right)(\rho_{MeO}/\rho_{Me})(r_{MeO}/r_{Me})^3 \tag{10}$$

where w, ρ and r are the weight percentage of MeO oxide in the mixture (see Table 1), density and radius of the particles (assumed to be spheres), respectively.

By taking $r_{MeO} = r_{Me}$ (i.e., a sharp grain size distribution for both the powders centred at a same value of r), R becomes equal to 13.3 and 2.4, for Ni(s)–NiO(s) and Fe(s)–$Fe_{1-\delta}O$(s) mixtures, respectively. Therefore, owing to the extensive mixing and pressing, each NiO and $Fe_{1-\delta}O$ particle should be surrounded by about 13 and 2 particle of metal, respectively. For NiO such a R value entails a compact assembly (the maximum number of spheres or radius, r, that can be arranged around a sphere of the same radius is 12, i.e., the fcc structure).

When the pressed mixture is heated, coalesc-

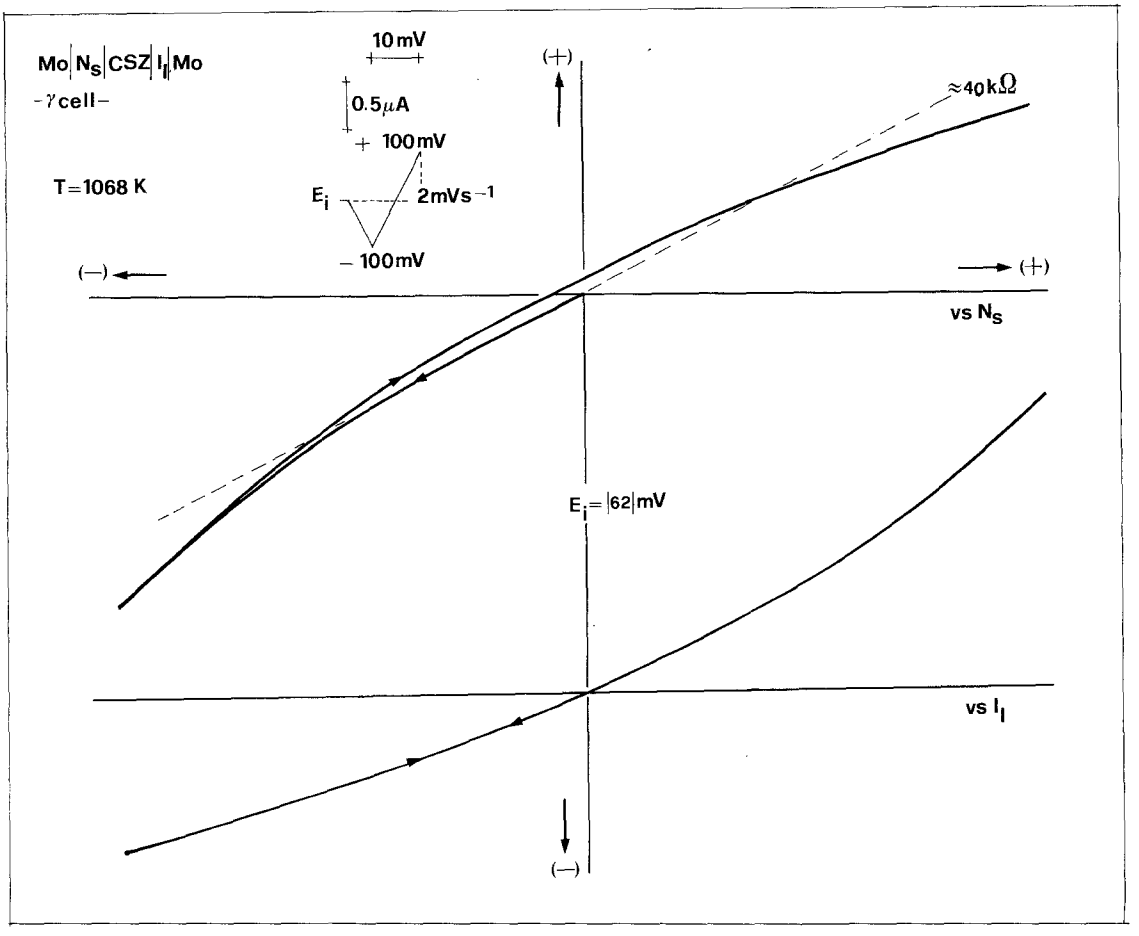

Fig. 4. Typical triangular wave voltammetry curves for a γ cell containing a N_S electrode.

ence of metal particle predominates for the following reasons [25]:

According to Tamman's rule, metals begin to sinter at 30–50% of their melting temperatures. Owing to their more rigid structures, oxides require 80–90% of their melting temperature. The situation is depicted in Fig. 7 where it is easy to see that at 1000° C the sintering of NiO is unfavourable while metals and $Fe_{1-\delta}O$ [26] may sinter.

The general condition for common sintering of heterogeneous particles, A and B, with respect to their surface energy, σ_A and σ_B, as compared with the surface energy between the two components, σ_{AB}, is $\sigma_{AB} < \sigma_A + \sigma_B$. Otherwise, no sintering between the two components will take place. There are still two further possibilities to be considered:

If $\sigma_{AB} > \sigma_A - \sigma_B$, the sintering will occur by the filling of the neck between the grains A and B and actual shrinkage of the grain centre distances occurs;

If $\sigma_{AB} < \sigma_A - \sigma_B$, the sintering begins with surface hetero-diffusion, leading to the coating of A by B. In this case, there will be a continuous phase B with the dispersed grains A, enveloped by B.

At first glance, the latter case seems to agree better for N_I samples, although it is very difficult to check the fulfilment of the above inequalities.

Data on surface tension of solids and especially surface energies between solids are lacking. The gas environment [27, 28] and the anisotropy of the surface energy [28] add further to the difficulties of putting values in those relations.

Brett and Seigle [29] have shown the predominant role of the diffusion flow mechanism in sintering with respect to plastic flow and found that in nickel wires containing 2% of dispersed

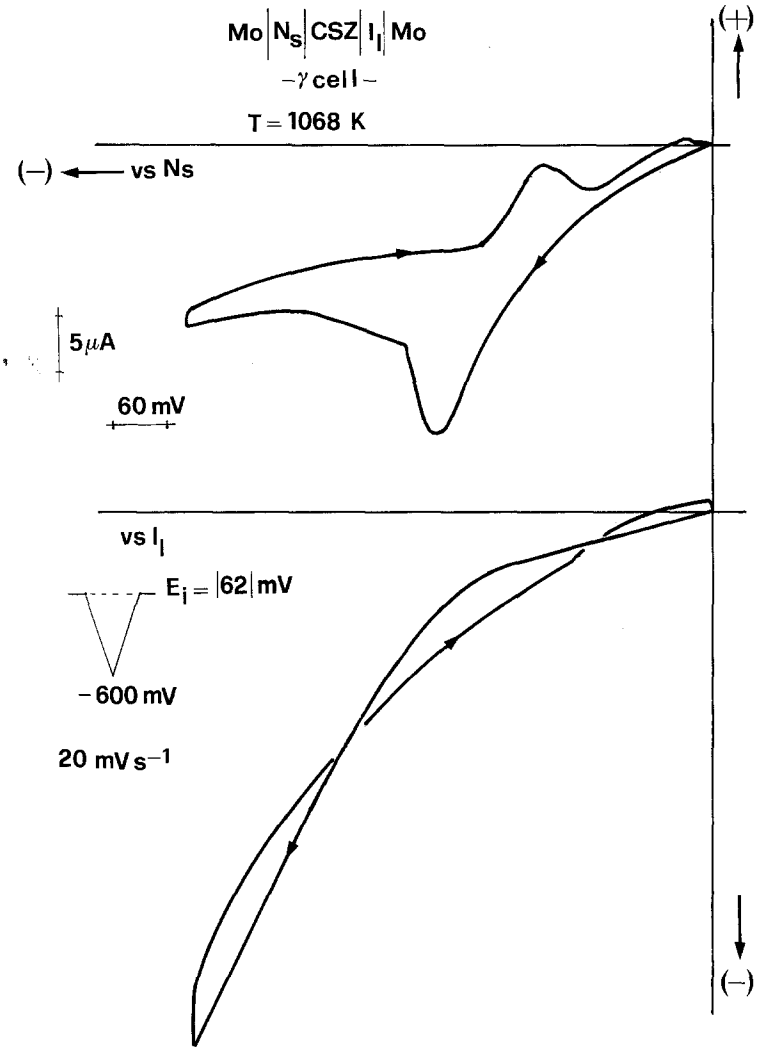

Fig. 5. Typical triangular wave voltammetry curves for a I_l and a N_s electrode.

alumina at 1400° C, only Ni was transferred to the necks and voids while Al_2O_3 behaved as an inert material.

By increasing the time of sintering, shrinkage of pores between nickel particles should occur by vacancy diffusion away from the interface under tension and by atom diffusion in the opposite direction. Ruczynski's review [30] explains well all aspects of this type of sintering mechanism which, briefly, in the case of powder sintering lies in the neck growing between two particles with an actual shrinkage of the specimen.

Rough density measurements of sintered pellets, both of I and of N types, showed the expected increase as a function of sintering time.

Since the Ni–O phase diagram [31] does not give an appreciable mutual solubility of NiO(s) and Ni(s), a possible explanation should be sought in the sintering mechanism according to the following ideal steps:

Coalescence of nickel around a NiO particle produces a pore volume shrinkage among nickel particles which generates an almost uniform compression (if the above fcc model is adopted) of the surface of a NiO particle. As shown, for example, by van Bueren and Nornstra [32], the volume of spherical pores, V_p, would decrease during sintering at the rate

$$dV_p/dt = -(8\pi\sigma\bar{V}/RT)D \qquad (11)$$

where σ, $\bar{V}$ and D are the surface energy in J m^{-2}, the molar volume in m^3 mol^{-1} and the self-

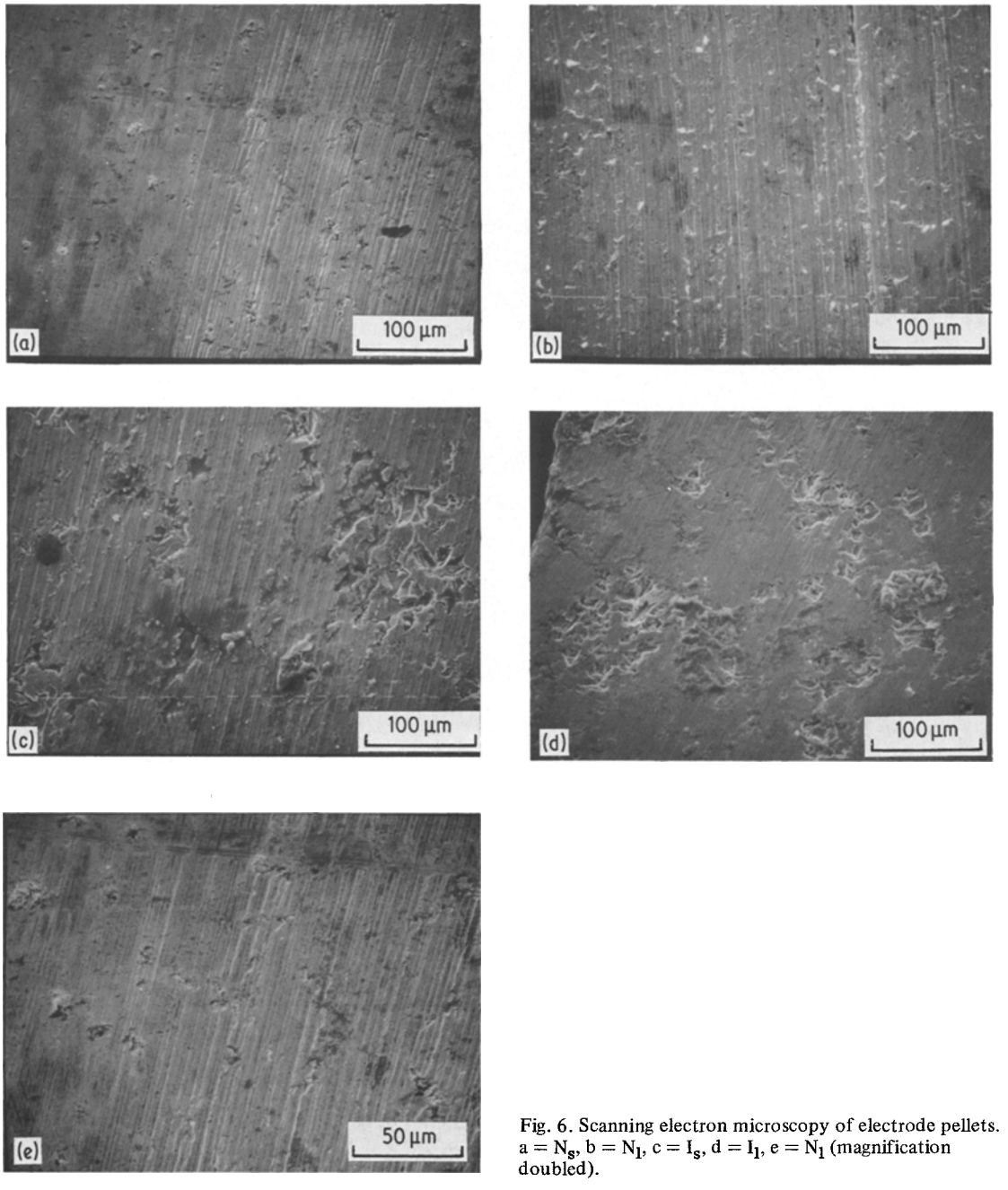

Fig. 6. Scanning electron microscopy of electrode pellets. a = N_s, b = N_l, c = I_s, d = I_l, e = N_l (magnification doubled).

diffusivity of the diffusing atom in $m^2 s^{-1}$. By assuming for nickel, $\sigma = 1.81\ J\ m^{-2}$ [28] (value at melting point) and D as given in Table 5, Equation 11, calculated at 1273 K, gives a dV_p/dt value of $-1.1 \times 10^{-23}\ m^3\ s^{-1}$.

If V_p is assumed as the volume occupied by a NiO particle, the tensile stress P acting on its surface (which tends to shrink the pore) is [30]

$$P = -2\sigma_{Ni}/r_p = -2\sigma_{Ni}(3V_p/4\pi)^{-1/3} \quad (12)$$

where r_p is the radius of the spherical pore (about the radius of a NiO particle). This stress, changing the sign, can be considered as the pressure applied by the shrinking nickel shell on the NiO particle producing an increase of its vapour pressure, P_v, with respect to the vapour pressure, P_v^0, in the

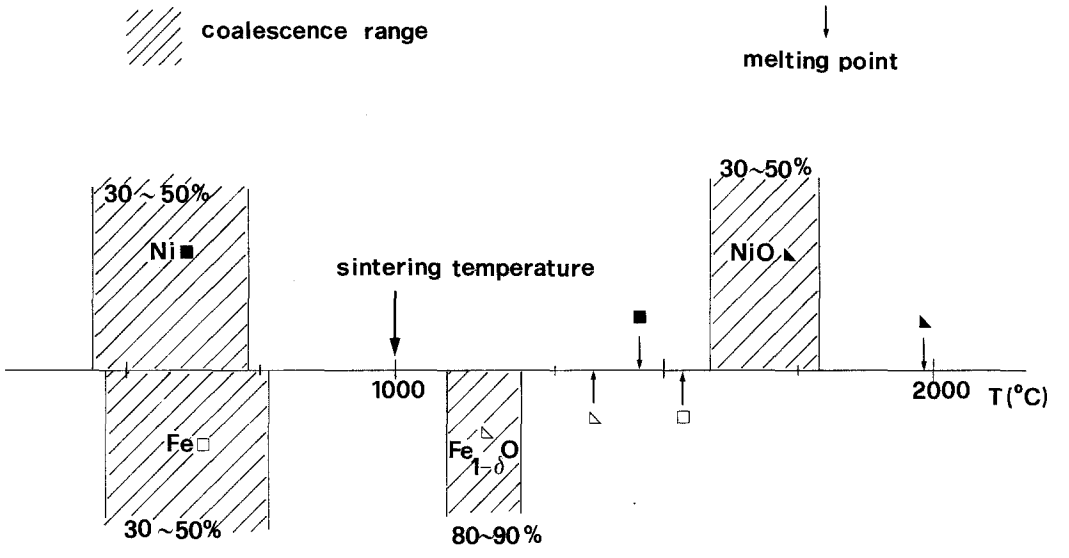

Fig. 7. Coalescence range for Fe, $Fe_{1-\delta}O$, Ni and NiO according to the Tamman's rule.

absence of compression, as given by the equation

$$\ln (P_v/P_v^0) = (\bar{V}_{NiO}/RT)P \qquad (13)$$

where, $\bar{V}_{NiO}$ is the molar volume of NiO in m^3mol^{-1}. By substituting Equation 12 in Equation 13 and taking the integrated form of Equation 11 into account, Equation 13 becomes

$$\ln (P_v/P_v^0) = 3.22(\bar{V}_{NiO}\sigma_{Ni}/RT) \times [V_0 - (dV_p/dt)t]^{-1/3} \qquad (14)$$

where V_0 is the pore volume at $t = 0$.

Because of the small value of dV_p/dt, a significant increase of NiO vapour pressure will be reached on the smallest NiO particles. For example, at $t = 50400$ s (14 h) and $T = 1273$ K, the vapour pressure will increase by 1.6×10^{-2}% and 0.36%, for particle diameter of 44 μm (325 mesh) and 1 μm.

Since the actual pressed mixture is certainly very far from that previously supposed, there are pores unfilled with NiO particles and NiO particles larger than 44 μm and smaller than 1 μm. The latter behave as a vapour source while the largest particles, or more likely the voids behave as condensation sites.

Table 5. Self-diffusion coefficient values for Ni and Fe. T = 1273 K

	D (cm^2s^{-1}) at 1273 K	Reference
Ni^{63}(Ni)	4.0×10^{-12}	34
Ni(NiO)	1.8×10^{-11}	4
$Fe^{58}(Fe_\gamma)$	1.1×10^{-12}	34
$Fe(Fe_{1-\delta}O)$	8.1×10^{-8}	4

In order to estimate the order of magnitude of NiO produced by evaporation, the Knudsen's equation can be applied for calculating the vapour mass effusing in one second from a hole of 2 μm diameter, for example.

By assuming a value of 1×10^{-3} Nm^{-2} [33] as the pressure of all vapour species in equilibrium with NiO(s) at 1273 K, the rate of effusion is of 3.4×10^{-15} gs^{-1}.

The average diameter of the NiO grains appearing in Fig. 6b is 5 μm, corresponding to a mass of 5×10^{-10} g. This value, assumed as the mass of condensed vapour effused from a single pore (NiO filled), can be obtained in a time of 1.4×10^5 s ($\simeq$ 40 h).

This time is about 3 times greater than the maximum sintering time adopted here, but more than one effusing flow may contribute to the growth of a NiO grain from the vapour phase.

Though other mechanisms could be considered, the final result would be, in any case, the isothermal 'transition' of NiO from a closed packing of nickel particles (Fig. 6a or 6e) to a compact metallic matrix embedding NiO grains (Fig. 6b). In the latter case, at the Ni(s)–NiO(s)/CSZ interface, triphasic coexistence is actually obtained whereas,

in the former case, only two phases (Ni(s) and O_2(g)) are in contact. This should not appreciably change the cell resistance as one can see in Fig. 3 and Fig. 4 (upper curves in both figures) where the cell resistance has been roughly estimated from the reciprocal value of the initial slope of the TWV curves.

As expected, owing to the higher value of iron diffusivity in $Fe_{1-\delta}O$ with respect to that of Ni in NiO (see Table 5) as well as the lower melting point of wüstite, a sintered Fe(s)–$Fe_{1-\delta}O$(s) mixture has good electrochemical properties.

Acknowledgements

The first author is grateful to Dr. M. Kleitz, ENSEEG-Grenoble, for the helpful discussion on this work on the occasion of Lithium Batteries Meeting in Rome. This work has been carried out by the financial support of the Centro di Termodinamica Chimica alle Alte Temperature, c/o Istituto di Chimica Fisica, Università di Roma, of the National Research Council of Italy (CNR).

References

[1] K. Kiukkola and C. Wagner, *J. Electrochem. Soc.* **104** (1957) 379.
[2] C. B. Alcock (ed.), 'Electromotive Force Measurements in High-temperature Systems', The Institute of Mining and Metallurgy, London (1968).
[3] R. A. Rapp and D. A. Shores in, 'Physicochemical Measurements in Metal Research', Part 2, Vol. 4, (edited by R. A. Rapp) Interscience, New York, (1970) Ch. 6.
[4] J. Hladik (ed.), 'Physics of Electrolytes', Vol. 2, Academic Press, London, (1972).
[5] S. N. Flengas, *High Temp. High Pressures* **5** (1973) 551.
[6] H. Schmalzried and A. D. Pelton, *Annu. Rev. of Mater. Sci.* **2** (1972) 143.
[7] T. A. Ramanarayanan and W. L. Worrel, *Can. Met. Q.* **13** (1974) 325.
[8] R. J. Fruehan, K. J. Martonik and E. T. Turkdogan, *Trans. AIME* **245** (1969) 1501.
[9] H. W. den Hartog and B. Slangen, *Ironmaking and Steelmaking* **2** (1976) 64.
[10] M. Iwase and T. Mori, *Trans. ISIJ* **19** (1979) 126.
[11] D. Gozzi, P. L. Cignini, E. Stampa, B. Alfonsi and M. Petrucci, *ibid.* **23** (1983).
[12] J. W. Patterson, *J. Electrochem. Soc.* **118** (1971) 1033.
[13] B. C. H. Steele in 'Electromotive Force Measurement in High Temperature Systems' (edited by C. B. Alcock) The Institute of Mining and Metallurgy. London (1968).
[14] H. Rickert, *ibid.*
[15] J. W. Patterson, E. C. Bogren and R. A. Rapp, *J. Electrochem. Soc.* **114** (1967) 752.
[16] F. J. Salzano, H. S. Isaacs and B. Minushkin, *ibid.* **118** (1971) 412.
[17] R. A. Rapp and F. Maak, *Acta Metall.* **10** (1962) 63.
[18] C. Diaz and F. D. Richardson, *Trans. Instn. Min. Metall.* **76C** (1967) 196.
[19] D. Gozzi, P. L. Cignini and E. Stampa, *Electrochim. Acta*, in press.
[20] O. Kubaschewski and C. B. Alcock, 'Metallurgical Thermochemistry', 5th Ed., Int. Series on Materials Science and Technology Vol. 24, (edited by G. V. Rainor) Pergamon Press, Oxford (1979).
[21] I. Barin and O. Knacke, 'Thermochemical Properties of Inorganic Substances', Springer, Berlin, (1973).
[22] Su-Il Pyun and F. Müller, *High Temp. High Pressures* **9** (1977) 111.
[23] K. Vetter, 'Electrochemical Kinetics', Academic Press, New York, (1967).
[24] P. Delahay, 'New Instrumental Methods in Electrochemistry', Interscience, New York, (1954).
[25] E. Ryshkewitch, 'Oxide Ceramics Physical Chemistry and Technology', Academic Press, New York, (1960).
[26] M. W. Pepper, K. Li and W. O. Philbrook, *Can. Met. Q.* **15** (1976) 201.
[27] E. D. Hondros and M. McLean, *C.N.R.S. Conf.* **187** (1969) 219.
[28] R. A. Swalin, 'Thermodynamics of Solids', 2nd Ed. John Wiley & Sons, New York, (1972).
[29] G. J. Brett and L. Seigle, *Acta Met.* **14** (1966) 575.
[30] G. C. Kuczynski, *Adv. Colloid. Interface Sci.* **3** (1972) 275.
[31] M. Hansen and K. Anderko, 'Constitution of Binary Alloys', 2nd Ed. McGraw-Hill, New York, (1958).
[32] H. G. van Bueren and J. Hornstra, in, 'Reactivity of Solids' (edited by J. H. De Boer) Elsevier, Amsterdam, (1961).
[33] R. T. Grimley, R. P. Burns and M. G. Inghram, *J. Chem. Phys.* **35** (1961) 551.
[34] J. Askill, 'Tracer Diffusion Data for Metals, Alloys and Simple Oxides' Plenum Press, New York, (1970).